Journal of Solid Mechanics Vol. 15, No. 2 (2023) pp. 198-216
DOI: 10.22034/jsm.2023.1970968.1755

Research Paper

Effect of Thermosensitivity on Heat Conduction and Stresses of a Multilayered Annular Disk

G.D. Kedar[1], V.B. Srinivas[1], V.R. Manthena [2,*]

[1]*Department of Mathematics, RTM Nagpur University, Nagpur, India*
[2]*Department of Mathematics, Priyadarshini J. L. Co1llege of Engineering, Nagpur, India*

Received 7 March 2023; accepted 3 May 2023

ABSTRACT

This paper deals with the analysis of temperature, deflection and thermal stresses of a multilayered annular disk. The thermo-mechanical properties of the disk are taken to be temperature dependent. Using Kirchhoff's variable transformation, the non-linear heat conduction equation is reduced to a linear form. Finite integral transform, Fourier series and Fourier transform techniques are used to solve the heat conduction equation and the desired solution is obtained in series form. Deflection, thermally induced resultant moments and the corresponding thermal stresses are determined. Numerical analysis is carried out for a three layered annular disk and the results are depicted graphically. Thermosensitivity plays a vital role in the thermal profile of the multilayered disk. In the temperature dependent case, the radial stress suddenly becomes compressive in the middle region, whereas it is tensile throughout all the regions in the temperature independent case. Due to the inhomogeneous thermal conductivity considered in the form of exponential function, the temperature and the corresponding thermoelastic quantities shows the lag along radial direction.

© 2023 IAU, Arak Branch.All rights reserved.

Keywords: Multilayered annular disk; Temperature dependent; Integral transform; Thermal deflection; Thermal stresses.

1 INTRODUCTION

IN thermo-mechanics, analysis of thermoelastic behavior in structural elements is important under manufacturing and operating conditions. Inhomogeneity in material structure in many cases occurs due to high and low level temperatures. Engineering application gives preference to the construction of solution of thermosensitive problems which is useful in production of stress bearing materials under the conditions of high temperature heating. Therefore the effect of thermosensitivity should be considered for investigation of heat conduction problems and the corresponding thermoelastic behavior. Thus to describe thermo-stressed state of the structure, a mathematical model is constructed by taking the dependency of the physiomechanical characteristics of the material on temperature.

*Corresponding author.
E-mail address: vkmanthena@gmail.com (V.R. Manthena)

© 2023 IAU, Arak Branch. All rights reserved.

Noda [1] discussed the effect of temperature dependent material properties on the thermal behavior of different solids. Olcer [2] discussed a complete analytical study for the distribution of temperature in a hollow right circular cylinder of finite length. Gorman [3] studied the effect of a radial parabolic temperature distribution upon the natural frequencies of small free transverse vibration (axi and non-axisymmetric) of polar orthotropic circular plates. Popovych et al. [4, 5] studied the heat conduction problems on various solids. Malzbender and Jülich [6] derived a general solution for elastic deformation of multilayered materials due to external loads and moments, mismatch in thermal expansion, and temperature gradients. Kayhani et al. [7] presented an exact general solution for steady-state conductive heat transfer in cylindrical composite laminates and obtained appropriate Fourier transformation using Sturm-Liouville theorem. Singh [8] discussed the methodology as well as possible application in nuclear reactors of analytical solutions of two-dimensional multilayer heat conduction in spherical and cylindrical coordinates. Singh et al. [9] used the finite integral transform method to determine the asymmetric heat conduction in a multilayer annulus. Kayhani et al. [10] presented a steady analytical solution for heat conduction in a cylindrical multilayer composite laminate and obtained the analytical solution for general linear boundary conditions that are suitable for various conditions including combinations of conduction, convection, and radiation both inside and outside the cylinder. Norouzi et al. [11] presented an exact analytical solution for steady conductive heat transfer in multilayer spherical fiber reinforced composite laminates. Dalir and Nourazar [12] presented an exact analytical solution of the problem on the three-dimensional transient heat conduction in a cylinder with multiple radial layers. Popovych and Kalynyak [13] developed a Mathematical model and analyzed the static thermoelastic behavior of multilayered thermally sensitive cylinder. Torabi and Zhang [14] determined the exact solution for asymmetric transient problem of heat conduction and accordingly thermal stresses within multilayer hollow or solid disks which lose heat by convection to the surrounding ambient. Manthena et al. [15, 16] obtained the thermal stresses of a nonhomogeneous hollow cylinder. Bhad et al. [17] studied the thermoelastic problem in multilayered elliptical composite plate with internal heat generation. Wang et al. [18] used asymptotic approach and studied the thermoelastic behavior of functionally graded (FG) thick hollow cylinder. Manthena et al. [19, 20, 21] studied thetemperature and stress profile of various solids subjected to temperature dependent material properties. Singh and Mukhopadhyay [22] studied thermoelastic interactions in an infinite homogeneous, isotropic elastic medium with a cylindrical cavity when the surface of the cavity is subjected to thermal shock. Zenkour [23] presented an exact solution of a thermal shock for a circular cylinder. Bhoyar et al. [24] investigated the transient thermoelastic reaction in a nonhomogeneous semielliptical elastic plate heated sectionally on the upper side of the semi-elliptic region. Bawankar and Kedar [25] developed a new model in magneto-thermoelasticity with modified Ohm's law in the form of the heat conduction equation with memory-dependent-derivative. Gheisari et al. [26] investigated the thermal buckling analysis of a truncated conical shell made of porous materials on elastic foundation. Dehghanpour et al. [27] investigated the factors affecting the diffusion bonding between the patch and the piece. Adolfsson [28] studied closed-form expressions for temperatures and elastic thermal stresses in an infinite hollow two-material compound cylinder subject to steady-periodic sinusoidal ambient temperatures. Mahakalkar and Varghese [29] developed an analytical framework for the thermoelastic analysis of annular sector plate. Mirparizi et al. [30] presented a finite element nonlinear coupled thermoelasticity formulation for analysis of the wave propagation, reflection, and mixing phenomena in the finite length isotropic solids. Hosseini et al. [31] presented a numerical solution for static and dynamic stability analysis of carbon nanotube reinforced beams resting on Pasternak foundation. Keshavarzian et al. [32] used Exponential Shear Deformation Theory to investigate the behavior of free vibrations of the thick sandwich panel with multi-layer face sheets and an electrorheological fluid core. Eslami et al. [33] analyzed the exact elasticity solution for a functionally graded circular shaft with piezo layers. Arani et al. [34] carried out dynamic stability analysis of bi-directional functionally graded materials. During the past three decades, due to the use of structural materials at extremely high temperatures, a trend of investigation of thermoelasticity is created in which the influence of temperature and mechanical properties of the structure is taken into consideration. Hence the study of thermal stresses in different solids with temperature dependent material properties has become important. Unsteady heat-conduction problems for homogeneous thermosensitive bodies can be completely linearized using the Kirchhoff variable when the temperature or heat flux is prescribed on the boundaries. However, the Kirchhoff variable partially linearises the heat-conduction problem in the cases of radiative, convective, or mixed heat transfer. In all these cases an additional linearization of the heat exchange, contact, or both must be performed in order to find the solution of the problem. Numerical methods are used to study temperature fields with heat transfer in homogeneous bodies whose thermophysical characteristics depend on the temperature. However, analytic solutions of such problems are needed for qualitative analysis to solve the corresponding problems of thermoelasticity.

In the present paper, the effect of thermosensitive material properties is studied on a multilayered annular circular disk occupying the space $r_{i-1} < r < r_i$, $0 < \theta < 2\pi$, $0 < z < h$, in context with thermal deflection and

© 2023 IAU, Arak Branch

thermally induced resultant moments. The temperature distribution is determined using integral transform technique. The effect of stress resultants on thermal stresses is studied. As a special case, numerical computations are carried out for a three-layered annular disk in which copper is selected as the inner layer, zinc as the middle layer and aluminium as the outer layer.

2 HEAT CONDUCTION EQUATION AND ITS SOLUTION

Consider a multilayered thin annular disk occupying the space $r_{i-1} < r < r_i$, $0 < \theta < 2\pi$, $0 < z < h$. The following Fig. 1. gives the geometrical representation of the multilayered annular disk.

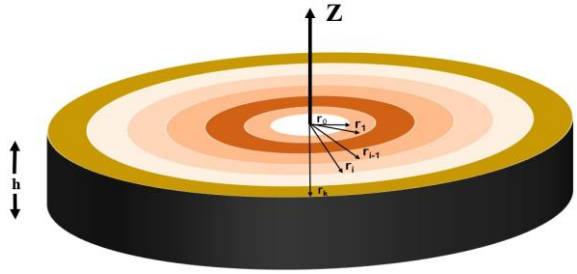

Fig.1
Geometrical representation of the multilayered annular circular disk.

The three dimensional transient state heat conduction equation (HCE) without heat source of a multilayered annular circular disk with temperature dependent material properties as modified from [21] is:

$$\frac{1}{r}\frac{\partial}{\partial r}\left(r\,\lambda_i(T_i)\frac{\partial T_i}{\partial r}\right)+\frac{1}{r^2}\frac{\partial}{\partial \theta}\left(\lambda_i(T_i)\frac{\partial T_i}{\partial \theta}\right)+\frac{\partial}{\partial z}\left(\lambda_i(T_i)\frac{\partial T_i}{\partial z}\right)=\rho_i\,C_i(T_i)\,\frac{\partial T_i}{\partial t} \tag{1}$$

where $\lambda_i(T_i), C_i(T_i)$ are respectively, the temperature dependent thermal conductivity, specific heat capacity of the *i*th layer, ρ_i is the density of the ith layer, and $i = 1,2,3,.....,k$.

Initial condition:

$$T_i = 0, \qquad \text{at } t = 0 \tag{2}$$

Boundary conditions:
Inner surface of the first layer ($i = 1$)

$$\lambda_1(T_1)\frac{\partial T_1}{\partial r}+h_0 T_1 = 0, \qquad \text{at } r = r_0 \tag{3}$$

Outer surface of the *k*th layer ($i = k$)

$$\lambda_k(T_k)\frac{\partial T_k}{\partial r}+h_k T_k = f_k(z,\theta,t), \qquad \text{at } r = r_k \tag{4}$$

Interface of the i*th* layer ($i = 2,3,.....,k$)

$$\begin{aligned} &T_i(r_{i-1},\theta,z,t) = T_{i-1}(r_{i-1},\theta,z,t) \\ &\lambda_i(T_i)\left.\frac{\partial T_i}{\partial r}\right|_{r=r_{i-1}} = \lambda_{i-1}(T_{i-1})\left.\frac{\partial T_{i-1}}{\partial r}\right|_{r=r_{i-1}} \end{aligned} \tag{5}$$

© 2023 IAU, Arak Branch

Periodic boundary conditions ($i = 1, 2, 3, \ldots\ldots\ldots\ldots, k$)

$$T_i\big|_{\theta=0} = T_i\big|_{\theta=2\pi}\ ,\quad \lambda_i(T_i)\left.\frac{\partial T_i}{\partial \theta}\right|_{\theta=0} = \lambda_i(T_i)\left.\frac{\partial T_i}{\partial \theta}\right|_{\theta=2\pi} \tag{6}$$

Boundary conditions along thickness

$$T_i = 0, \qquad \text{at } z = 0,\ h \tag{7}$$

where $h_0,\ h_k$ are the surface coefficients at $r = r_0,\ r = r_k$. We use following dimensionless parameters.

$$\begin{aligned} &T_i^* = \frac{T_i}{T_0},\ r^* = \frac{r}{h},\ \theta^* = \frac{\theta}{2\pi},\ z^* = \frac{z}{h},\ t^* = \frac{\kappa_1 t}{h^2}\ ,\ \rho_i^* = \frac{\rho_i}{\rho_1},\ (r_i^*, h^*) = \frac{(r_i, h)}{h},\ E_i^* = \frac{E_i}{E_1},\\ &a^* = \frac{a\,h^2}{\kappa_1}, \varpi_j^* = \frac{\varpi_j\, h^2}{\kappa_1},\ j = 1, 2. \end{aligned} \tag{8}$$

where T_0 is the temperature of the surrounding environment, h is the thickness of the disk, $\kappa_1 = \lambda_1/(C_1\rho_1),$ is the thermal diffusivity of the inner layer, λ_1, C_1, ρ_1 are the thermal conductivity, specific heat capacity, density of the inner layer, E_i is the Young's modulus, a, ϖ_j are the frequency.

The temperature dependent material properties $\lambda_i(T_i), C_i(T_i)$, and heat flow $f_k(z, \theta, t)$ are taken as [4, 5]

$$\begin{aligned} &\lambda_i(T_i) = \lambda_1 \lambda_i^*(T_i^*)\\ &C_i(T_i) = C_1 C_i^*(T_i^*)\\ &f_k(z, \theta, t) = f_0 f_k^*(z^*, \theta^*, t^*) \end{aligned} \tag{9}$$

where λ_1, C_1 have dimensions, f_0 is the strength of the heat flow having relevant dimension, and $\lambda_i^*(T_i^*), C_i^*(T_i^*)$ are the dimensionless quantities, which are functions that describe the dependence of these characteristics on dimensionless temperature, $f_k^*(z^*, \theta^*, t^*)$ is the dimensionless function which describes the space distribution of the heat flow. Using Eqs. (8-9), Eqs. (1-7) reduces to the following dimensionless form (ignoring asterisks for convenience).

$$\frac{1}{r}\frac{\partial}{\partial r}\left(r\,\lambda_i(T_i)\frac{\partial T_i}{\partial r}\right) + \frac{1}{4\pi^2 r^2}\frac{\partial}{\partial \theta}\left(\lambda_i(T_i)\frac{\partial T_i}{\partial \theta}\right) + \frac{\partial}{\partial z}\left(\lambda_i(T_i)\frac{\partial T_i}{\partial z}\right) = \rho_i\, C_i(T_i)\,\frac{\partial T_i}{\partial t} \tag{10}$$

Initial condition:

$$T_i = 0, \qquad \text{at } t = 0 \tag{11}$$

Boundary conditions:
Inner surface of the first layer ($i = 1$)

$$\lambda_1(T_1)\frac{\partial T_1}{\partial r} + Bi_1 T_1 = 0, \qquad \text{at } r = \Phi_1 \tag{12}$$

Outer surface of the kth layer ($i = k$)

$$\lambda_k(T_k)\frac{\partial T_k}{\partial r} + Bi_2 T_k = Ki\, f_k(z, \theta, t), \qquad \text{at } r = \Phi_2 \tag{13}$$

© 2023 IAU, Arak Branch

Interface of the i*th* layer ($i = 2, 3, ..., k$)

$$T_i(r_{i-1}, \theta, z, t) = T_{i-1}(r_{i-1}, \theta, z, t)$$
$$\lambda_i(T_i) \left.\frac{\partial T_i}{\partial r}\right|_{r=r_{i-1}} = \lambda_{i-1}(T_{i-1}) \left.\frac{\partial T_{i-1}}{\partial r}\right|_{r=r_{i-1}} \tag{14}$$

Periodic boundary conditions ($i = 1, 2, 3, ..., k$)

$$T_i\big|_{\theta=0} = T_i\big|_{\theta=1},$$
$$\lambda_i(T_i) \left.\frac{\partial T_i}{\partial \theta}\right|_{\theta=0} = \lambda_i(T_i) \left.\frac{\partial T_i}{\partial \theta}\right|_{\theta=1} \tag{15}$$

Boundary conditions along thickness

$$T_i = 0, \qquad \text{at } z = 0,\ h \tag{16}$$

where $Ki = \dfrac{f_0 h}{\lambda_1 T_0}$ is the dimensionless Kirpichev reference number, $Bi_1 = \dfrac{h_0 h}{\lambda_1}$, $Bi_2 = \dfrac{h_k h}{\lambda_1}$ are the Biot criteria, $\Phi_1 = (r_0 / h),\ \Phi_2 = (r_k / h)$.

Introducing Kirchhoff's variable transformation [4, 5, 13]

$$\Theta_i(T_i) = \int_o^{T_i} \lambda_i(T_i)\, d\,T_i \tag{17}$$

and considering the material with simple thermal nonlinearity (that is $[C_i(T_i) / \lambda_i(T_i)] \approx 1$), Eqs. (10) to (16) become

$$\frac{\partial^2 \Theta_i}{\partial r^2} + \frac{1}{r}\frac{\partial \Theta_i}{\partial r} + \frac{1}{4\pi^2 r^2}\frac{\partial^2 \Theta_i}{\partial \theta^2} + \frac{\partial^2 \Theta_i}{\partial z^2} = \rho_i \frac{\partial \Theta_i}{\partial t} \tag{18}$$

Initial condition:

$$\Theta_i = 0, \qquad \text{at } t = 0 \tag{19}$$

Boundary conditions:
Inner surface of the first layer ($i = 1$)

$$\frac{\partial \Theta_1}{\partial r} + Bi_1\, \Theta_1 = 0, \qquad \text{at } r = \Phi_1 \tag{20}$$

Outer surface of the *k*th layer ($i = k$)

$$\frac{\partial \Theta_k}{\partial r} + Bi_2\, \Theta_k = Ki\, f_k(z, \theta, t), \qquad \text{at } r = \Phi_2 \tag{21}$$

Interface of the i*th* layer ($i = 2, 3, ..., k$)

© 2023 IAU, Arak Branch

$$\Theta_i(r_{i-1},\theta,z,t)=\Theta_{i-1}(r_{i-1},\theta,z,t)$$
$$\left.\frac{\partial\Theta_i}{\partial r}\right|_{r=r_{i-1}}=\left.\frac{\partial\Theta_{i-1}}{\partial r}\right|_{r=r_{i-1}} \tag{22}$$

Periodic boundary conditions ($i=1,2,3,.....,k$)

$$\Theta_i\big|_{\theta=0}=\Theta_i\big|_{\theta=1}$$
$$\left.\frac{\partial\Theta_i}{\partial\theta}\right|_{\theta=0}=\left.\frac{\partial\Theta_i}{\partial\theta}\right|_{\theta=1} \tag{23}$$

Boundary conditions along thickness

$$\Theta_i=0, \qquad \text{at } z=0,\ h \tag{24}$$

For the sake of brevity, we take $f_k(\theta,z,t)=\delta(\theta-\theta_0)\delta(z-z_0)\exp(at)$. Here $f_k(\theta,z,t)$ represents an exponentially varying point heat, θ_0 , z_0 being dimensionless constants. Using finite Fourier Sine transform on Eqs. (18) and (24) over the variable z , yields

$$\frac{\partial^2\bar{\Theta}_i}{\partial r^2}+\frac{1}{r}\frac{\partial\bar{\Theta}_i}{\partial r}+\frac{1}{4\pi^2r^2}\frac{\partial^2\bar{\Theta}_i}{\partial\theta^2}-\psi_n^2\bar{\Theta}_i=\rho_i\frac{\partial\bar{\Theta}_i}{\partial t} \tag{25}$$

The conditions (19-23) become

$$\bar{\Theta}_i=0, \qquad \text{at } t=0 \tag{26}$$

Inner surface of the first layer ($i=1$)

$$\frac{\partial\bar{\Theta}_1}{\partial r}+Bi_1\bar{\Theta}_1=0, \qquad \text{at } r=\Phi_1 \tag{27}$$

Outer surface of the *k*th layer ($i=k$)

$$\frac{\partial\bar{\Theta}_k}{\partial r}+Bi_2\bar{\Theta}_k=\bar{f}_k(\psi_n,\theta,t), \qquad \text{at } r=\Phi_2 \tag{28}$$

Interface of the *i*th layer ($i=2,3,.....,k$)

$$\bar{\Theta}_i(r_{i-1},\theta,\psi_n,t)=\bar{\Theta}_{i-1}(r_{i-1},\theta,\psi_n,t)$$
$$\left.\frac{\partial\bar{\Theta}_i}{\partial r}\right|_{r=r_{i-1}}=\left.\frac{\partial\bar{\Theta}_{i-1}}{\partial r}\right|_{r=r_{i-1}} \tag{29}$$

Periodic boundary conditions ($i=1,2,3,.....,k$)

$$\bar{\Theta}_i\big|_{\theta=0}=\bar{\Theta}_i\big|_{\theta=1}$$
$$\left.\frac{\partial\bar{\Theta}_i}{\partial\theta}\right|_{\theta=0}=\left.\frac{\partial\bar{\Theta}_i}{\partial\theta}\right|_{\theta=1} \tag{30}$$

© 2023 IAU, Arak Branch

where $\psi_n = n\pi/h, \bar{f}_k(\psi_n,\theta,t) = Ki\, z_0 \sin(n\pi z_0/h)\delta(\theta-\theta_0)\exp(at)$. The kernel of the transform is $\sin(n\pi z/h)$.

2.1 Eigen function expansion in θ direction

Because of periodic boundary conditions in θ direction, we expand $\bar{\Theta}_i(r,\theta,t)$ into angular eigen functions $\cos(m\theta)$, $\sin(m\theta)$ and a constant as follows [9]

$$\bar{\Theta}_i(r,\theta,t) = \bar{\Theta}_{i0}(r,t) + \sum_{m=1}^{\infty} \bar{\Theta}_{imc}(r,t)\cos(m\theta) + \sum_{m=1}^{\infty} \bar{\Theta}_{ims}(r,t)\sin(m\theta) \tag{31}$$

Similarly, the expression for heat supply is taken as:

$$\bar{f}_k(\theta,t) = \bar{f}_{k0}(\theta,t) + \sum_{m=1}^{\infty} \bar{f}_{kmc}(\theta,t)\cos(m\theta) + \sum_{m=1}^{\infty} \bar{f}_{kms}(\theta,t)\sin(m\theta) \tag{32}$$

Using the orthogonality conditions along θ direction, the coefficients in Eq. (32) are obtained as:

$$\begin{aligned}
\bar{f}_{i0}(r,t) &= \int_0^1 \bar{f}_i(r,\theta,t)\,d\theta \\
\bar{f}_{imc}(r,\theta,t) &= \int_0^1 \bar{f}_i(r,\theta,t)\cos(m\theta)\,d\theta \\
\bar{f}_{ims}(r,\theta,t) &= \int_0^1 \bar{f}_i(r,\theta,t)\sin(m\theta)\,d\theta
\end{aligned} \tag{33}$$

Using Eqs. (31) and (32) in Eqs. (25) and (30), we obtain [omitting the subscripts $0, c, s$]

$$\left(\frac{\partial^2\bar{\bar{\Theta}}_{im}}{\partial r^2} + \frac{1}{r}\frac{\partial\bar{\bar{\Theta}}_{im}}{\partial r} - \frac{m^2}{4\pi^2 r^2}\bar{\bar{\Theta}}_{im} - \psi_n^2\bar{\bar{\Theta}}_{im}\right) = \rho_i\frac{\partial\bar{\bar{\Theta}}_{im}}{\partial t} \tag{34}$$

The conditions (26-29) become

$$\bar{\bar{\Theta}}_{im} = 0, \qquad \text{at } t = 0 \tag{35}$$

Inner surface of the first layer ($i = 1$)

$$\frac{\partial\bar{\bar{\Theta}}_{1m}}{\partial r} + Bi_1\bar{\bar{\Theta}}_{1m} = 0, \qquad \text{at } r = \Phi_1 \tag{36}$$

Outer surface of the kth layer ($i = k$)

$$\frac{\partial\bar{\bar{\Theta}}_{km}}{\partial r} + Bi_2\bar{\bar{\Theta}}_{km} = \bar{\bar{f}}_{km}(t), \qquad \text{at } r = \Phi_2 \tag{37}$$

Interface between the ith and (i-1)th layer ($i = 2, 3, \ldots\ldots\ldots\ldots, k$)

© 2023 IAU, Arak Branch

$$\bar{\bar{\Theta}}_{im}(r_{i-1},t)=\bar{\bar{\Theta}}_{i-1,m}(r_{i-1},t)$$
$$\left.\frac{\partial\bar{\bar{\Theta}}_{im}}{\partial r}\right|_{r=r_{i-1}}=\left.\frac{\partial\bar{\bar{\Theta}}_{i-1,m}}{\partial r}\right|_{r=r_{i-1}} \tag{38}$$

where $\bar{\bar{f}}_{km}(t)=A_1\exp(at)$, $A_1=Ki\,\theta_0 z_0\sin(m\,\theta_0/2)\sin(n\,\pi z_0/h)$.

2.2 Finite integral transform in the r-direction

Following [9], we operate Eq. (34) by $\int_{r_{i-1}}^{r_i} r\,S_{im}(r)dr$, and using integration by parts twice on the first term on the left hand side (LHS), yields

$$\int_{r_{i-1}}^{r_i}\left(\frac{\partial^2 S_{im}(r)}{\partial r^2}+\frac{1}{r}\frac{\partial S_{im}(r)}{\partial r}-\frac{m^2}{4\pi^2 r^2}S_{im}(r)-\psi_n^2 S_{im}(r)\right)r\,\bar{\bar{\Theta}}_{im}\,dr+\left[r\,S_{im}(r)\frac{\partial\bar{\bar{\Theta}}_{im}}{\partial r}-r\,\bar{\bar{\Theta}}_{im}\,\frac{\partial S_{im}(r)}{\partial r}\right]_{r_{i-1}}^{r_i}$$
$$=\int_{r_{i-1}}^{r_i}\left(\rho_i\frac{\partial\bar{\bar{\Theta}}_{im}}{\partial t}\right)r\,S_{im}(r)dr \tag{39}$$

$S_{im}(r)$ in Eq. (39) is chosen so that it satisfies the following differential equation

$$\frac{\partial^2 S_{im}(r)}{\partial r^2}+\frac{1}{r}\frac{\partial S_{im}(r)}{\partial r}+\left(-\frac{m^2}{4\pi^2 r^2}-\psi_n^2+\alpha_{im}^2\right)S_{im}(r)=0 \tag{40}$$

Boundary conditions:
Inner surface of the first layer ($i=1$)

$$\frac{dS_{1m}}{dr}+Bi_1 S_{1m}=0 \tag{41}$$

Outer surface of the *k*th layer ($i=k$)

$$\frac{dS_{km}}{dr}+Bi_2 S_{km}=0 \tag{42}$$

Interface between the *i*th and (*i*-1)th layer ($i=2,3,.....,k$)

$$S_{im}(r_{i-1})=S_{i-1,m}(r_{i-1})$$
$$\left.\frac{dS_{im}}{dr}\right|_{r=r_{i-1}}=\left.\frac{dS_{i-1,m}}{dr}\right|_{r=r_{i-1}} \tag{43}$$

The solutions of above equations are the eigen functions $S_{imp}(r)$ corresponding to the eigen values α_{imp} and are given by $S_{imp}(\alpha_{imp}r)=a_{imp}J_0(\alpha_{imp}r)+b_{imp}Y_0(\alpha_{imp}r)$, where J_0 and Y_0 are Bessel's function of first kind and second kind respectively, and a_{imp}, b_{imp} are arbitrary constants. The eigen function α_{imp} satisfies the following orthogonality condition (44) subject to (45)

© 2023 IAU, Arak Branch

$$\sum_{i=1}^{k} \int_{r_{i-1}}^{r_i} r\, S_{imp}(\alpha_{imp}\, r) S_{imp}(\alpha_{imq}\, r)\, dr = \begin{vmatrix} 0\,; & p \neq q \\ S_{imp}(\alpha_{imp})\,; & p = q \end{vmatrix} \tag{44}$$

$$\kappa_i \alpha_{imp}^2 = \kappa_1 \alpha_{1mp}^2 \tag{45}$$

Using Eq. (40), Eq. (39) becomes

$$\left[r\, S_{imp}(r) \frac{\partial \bar{\bar{\Theta}}_{im}}{\partial r} - r\, \bar{\bar{\Theta}}_{im} \frac{\partial S_{imp}(r)}{\partial r} \right]_{r_{i-1}}^{r_i} = \int_{r_{i-1}}^{r_i} \left(\rho_i \frac{\partial \bar{\bar{\Theta}}_{im}}{\partial t} + \alpha_{imp}^2 \bar{\bar{\Theta}}_{im} \right) r\, S_{imp}(r)\, dr \tag{46}$$

Using Eq. (45), Eq. (46) becomes

$$\left[r\, S_{imp}(r) \frac{\partial \bar{\bar{\Theta}}_{im}}{\partial r} - r\, \bar{\bar{\Theta}}_{im} \frac{\partial S_{imp}(r)}{\partial r} \right]_{r_{i-1}}^{r_i} = \int_{r_{i-1}}^{r_i} \left(\rho_i \frac{\partial \bar{\bar{\Theta}}_{im}}{\partial t} + (\kappa_1 / \kappa_i) \alpha_{1mp}^2 \bar{\bar{\Theta}}_{im} \right) r\, S_{imp}(r)\, dr \tag{47}$$

Multiplying the above equation by λ_i and summing over all the *k* layers, we obtain

$$\sum_{i=1}^{k} \lambda_i \left[r\, S_{imp}(r) \frac{\partial \bar{\bar{\Theta}}_{im}}{\partial r} - r\, \bar{\bar{\Theta}}_{im} \frac{\partial S_{imp}(r)}{\partial r} \right]_{r_{i-1}}^{r_i} = \sum_{i=1}^{k} \int_{r_{i-1}}^{r_i} \lambda_i \left(\rho_i \frac{\partial \bar{\bar{\Theta}}_{im}}{\partial t} + (\kappa_1 / \kappa_i) \alpha_{1mp}^2 \bar{\bar{\Theta}}_{im} \right) r\, S_{imp}(r)\, dr \tag{48}$$

We define

$$\bar{\bar{\Theta}}_{mp}^{\phi} = \sum_{i=1}^{k} \lambda_i \int_{r_{i-1}}^{r_i} r\, S_{imp}(r)\, \bar{\bar{\Theta}}_{im}\, dr \tag{49}$$

Hence Eq.(48) becomes

$$\rho_i \frac{d\, \bar{\bar{\Theta}}_{mp}^{\phi}}{d\, t} + (\kappa_1 / \kappa_i) \alpha_{1mp}^2 \bar{\bar{\Theta}}_{mp}^{\phi} = \sum_{i=1}^{k} \lambda_i \left[r\, S_{imp}(r) \frac{\partial \bar{\bar{\Theta}}_{im}}{\partial r} - r\, \bar{\bar{\Theta}}_{im} \frac{\partial S_{imp}(r)}{\partial r} \right]_{r_{i-1}}^{r_i} \tag{50}$$

Applying the interface conditions (38) and (43), yields

$$\frac{d\, \bar{\bar{\Theta}}_{mp}^{\phi}}{d\, t} + A_2 \bar{\bar{\Theta}}_{mp}^{\phi} = A_3 \exp(at) \tag{51}$$

where $A_2 = (\kappa_1 / \rho_i\, \kappa_i)\, \alpha_{1mp}^2$, $A_3 = A_1 (\lambda_k\, r_k / \rho_k)$. The initial condition is

$$\bar{\bar{\Theta}}_{mp}^{\phi} = 0, \qquad \text{at } t = 0 \tag{52}$$

Applying Laplace transform and its inverse on Eqs. (51) and (52), yields

$$\bar{\bar{\Theta}}_{mp}^{\phi} = E_1 [\exp(at) - \exp(-A_2 t)] \tag{53}$$

where $E_1 = (A_3 / A_2 + a)$.

© 2023 IAU, Arak Branch

2.3 Inversion formula

The generalized Fourier series expansion of $\bar{\bar{\Theta}}_{im}(r,t)$ is as follows:

$$\bar{\bar{\Theta}}_{im}(r,t)=\sum_{p=1}^{\infty} c_{mp}(t)S_{imp}(r) \tag{54}$$

where $c_{mp}(t)=[\sum_{i=1}^{k} \lambda_i \int_{r_{i-1}}^{r_i} r S_{imp}(r)\bar{\bar{\Theta}}_{im}\,dr]/[S_{imp}(\alpha_{imp})]$. Now using Eq. (49), we get $c_{mp}(t)=[\bar{\bar{\Theta}}^{\phi}_{mp}]/[S_{imp}(\alpha_{imp})]$. This formulation and solution is valid only for $\bar{\Theta}_{i0}(r,t)$, $\bar{\Theta}_{imc}(r,t)$, $\bar{\Theta}_{ims}(r,t)$ in Eq. (31). Using Eq. (54) in Eq. (31), we get

$$\bar{\Theta}_i(r,\theta,t)=\sum_{p=1}^{\infty} \Psi_2 S_{i0p}(r)+\sum_{m=1}^{\infty}\sum_{p=1}^{\infty} \Psi_3 S_{imp}(r)\cos(m\theta)+\sum_{m=1}^{\infty}\sum_{p=1}^{\infty} \Psi_4 S_{imp}(r)\sin(m\theta) \tag{55}$$

where $\Psi_2=[\bar{\bar{\Theta}}^{\phi}_{0p}]/[S_{i0p}(\alpha_{i0p})]$, $\Psi_3=[\bar{\bar{\Theta}}^{\phi}_{mpc}]/[S_{imp}(\alpha_{imp})]$, $\Psi_4=[\bar{\bar{\Theta}}^{\phi}_{mps}]/[S_{imp}(\alpha_{imp})]$.

Applying inverse Fourier Sine transform on the above Eq. (55), yields

$$\begin{aligned}\Theta_i(r,z,\theta,t)=\sum_{n=1}^{\infty}\{&\sum_{p=1}^{\infty} \Psi_2 S_{i0p}(r)+\sum_{m=1}^{\infty}\sum_{p=1}^{\infty} \Psi_3 S_{imp}(r)\cos(m\theta)\\&+\sum_{m=1}^{\infty}\sum_{p=1}^{\infty} \Psi_4 S_{imp}(r)\sin(m\theta)\}\sin(n\pi z/h)\end{aligned} \tag{56}$$

Following Noda [1], the temperature dependent thermal conductivity is expressed as an exponential function of temperature as:

$$\lambda_i(T_i)=\lambda_{i0}\exp(\varpi_1 T_i),\ \varpi_1\le 0 \tag{57}$$

Here λ_{i0} is the dimensionless reference value of thermal conductivity defined by, $\lambda_{i0}{}^{*}=\dfrac{\lambda_{i0}}{\lambda_{(i-1)0}}$. Substituting Eq.(57) in Eq.(17), yields

$$\Theta_i=(\lambda_{i0}/\varpi_1)[\exp(\varpi_1 T_i)-1] \tag{58}$$

Using Eq. (58) in Eq. (56), yields

$$T_i(r,z,\theta,t)=(1/\varpi_1)\log_e[g(r,z,\theta,t)+1] \tag{59}$$

where

$$\begin{aligned}g(r,z,\theta,t)=\sum_{n=1}^{\infty}(\varpi_1/\lambda_{i0})\{&\sum_{p=1}^{\infty} \Psi_2 S_{i0p}(r)+\sum_{m=1}^{\infty}\sum_{p=1}^{\infty} \Psi_3 S_{imp}(r)\cos(m\theta)\\&+\sum_{m=1}^{\infty}\sum_{p=1}^{\infty} \Psi_4 S_{imp}(r)\sin(m\theta)\}\sin(n\pi z/h)\end{aligned}$$

We use the following logarithmic expansion

© 2023 IAU, Arak Branch

$$\log_e[g(r,z,\theta,t)+1] = [g(r,z,\theta,t)]+(1/2)[g(r,z,\theta,t)]^2+(1/3)[g(r,z,\theta,t)]^3+..... \tag{60}$$

We observe that $[g(r,z,\theta,t)]^L$ given in Eq. (60) converges to zero as L tends to infinity. Also the truncation error in Eq. (60) is observed as 2.127×10^{-6}. Hence, for the sake of brevity, neglecting the terms with order more than one, yields $\log_e[g(r,z,\theta,t)+1] = g(r,z,\theta,t)$. Hence Eq. (59) becomes

$$\begin{aligned} T_i(r,z,\theta,t) = \sum_{n=1}^{\infty}(1/\lambda_{i0})\{\sum_{p=1}^{\infty}\Psi_2 S_{i0p}(r)+\sum_{m=1}^{\infty}\sum_{p=1}^{\infty}\Psi_3 S_{imp}(r)\cos(m\theta) \\ +\sum_{m=1}^{\infty}\sum_{p=1}^{\infty}\Psi_4 S_{imp}(r)\sin(m\theta)\}\sin(n\pi z/h) \end{aligned} \tag{61}$$

3 THERMOELASTIC ANALYSIS

In the cylindrical coordinate system, the fundamental equation and the boundary conditions for a simply supported thin annular disk under thermal load are [31]

$$\nabla^2\nabla^2 w^{(i)} = \frac{-1}{(1-\nu_i)D_i}\nabla^2 M_T^{(i)} \tag{62}$$

where

$$\nabla^2 = \frac{\partial^2}{\partial r^2}+\frac{1}{r}\frac{\partial}{\partial r}+\frac{1}{r^2}\frac{\partial^2}{\partial\theta^2}, \qquad D_i = \frac{E_i\ h^3}{12(1-\nu_i^2)} \tag{63}$$

Here $w^{(i)}$ is the deflection of the ith layer, $M_T^{(i)}$ is the thermally induced resultant moment of the ith layer, D_i, E_i and ν_i are respectively, the bending rigidity, Young's modulus and Poisson's ratio of the plate, which are assumed to be constant.

We restrict the problem to the case of symmetrical deflection so that the deflection depends only on radius and time. The initial and boundary conditions are

$$w^{(i)} = \frac{\partial w^{(i)}}{\partial t} = 0, \qquad \text{at } t=0 \tag{64}$$

The problem is restricted under thermal load by an elastic reaction along the boundaries $r=r_0$, $r=r_k$, so that the deflection satisfies the following continuity and boundary conditions [17, 21]

$$\begin{aligned} &\frac{\partial w^{(i)}}{\partial r}+w^{(i)} = 0, && \text{at } r=r_0, \\ &\frac{\partial w^{(k)}}{\partial r}+w^{(k)} = 0, && \text{at } r=r_k, \\ &w^{(i)} = w^{(i-1)} && \text{at } r=r_{i-1}, \\ &\frac{\partial w^{(i)}}{\partial r} = \frac{\partial w^{(i-1)}}{\partial r} && \text{at } r=r_{i-1}. \end{aligned} \tag{65}$$

The proportionality constants given by Hooke's law are assumed to be unity. The components of resultant forces, shearing forces and resultant moments are [31]

© 2023 IAU, Arak Branch

$$N_{rr}^{(i)} = N_{\theta\theta}^{(i)} = N_{r\theta}^{(i)} = 0 \tag{66}$$

$$\begin{aligned} Q_{rr}^{(i)} &= -D_i \frac{\partial}{\partial r}(\nabla^2 w^{(i)}) - \frac{1}{1-\nu_i}\frac{\partial M_T^{(i)}}{\partial r} \\ Q_{\theta\theta}^{(i)} &= -D_i \frac{1}{r}\frac{\partial}{\partial \theta}(\nabla^2 w^{(i)}) - \frac{1}{1-\nu_i}\frac{1}{r}\frac{\partial M_T^{(i)}}{\partial \theta} \end{aligned} \tag{67}$$

$$\begin{aligned} M_{rr}^{(i)} &= -D_i \left[\frac{\partial^2 w^{(i)}}{\partial r^2} + \frac{\nu_i}{r}\frac{\partial w^{(i)}}{\partial r}\right] - \frac{1}{1-\nu_i} M_T^{(i)} \\ M_{\theta\theta}^{(i)} &= -D_i \left[\nu_i \frac{\partial^2 w^{(i)}}{\partial r^2} + \frac{1}{r}\frac{\partial w^{(i)}}{\partial r}\right] - \frac{1}{1-\nu_i} M_T^{(i)} \end{aligned} \tag{68}$$

Here $M_{rr}^{(i)}$ satisfies the condition

$$M_{rr}^{(i)}\Big|_{r=r_0} = 0 \quad , \; 0 < \theta < 1 \tag{69}$$

The stress components in terms of resultant moments are

$$\begin{aligned} \sigma_{rr}^{(i)} &= \frac{1}{h} N_{rr}^{(i)} + \frac{12z}{h^3} M_{rr}^{(i)} + \frac{1}{1-\nu_i}\left(\frac{1}{h} N_T^{(i)} + \frac{12z}{h^3} M_T^{(i)} - \alpha_i (T_i)\, E_i\, T_i\right) \\ \sigma_{\theta\theta}^{(i)} &= \frac{1}{h} N_{\theta\theta}^{(i)} + \frac{12z}{h^3} M_{\theta\theta}^{(i)} + \frac{1}{1-\nu_i}\left(\frac{1}{h} N_T^{(i)} + \frac{12z}{h^3} M_T^{(i)} - \alpha_i (T_i)\, E_i\, T_i\right) \end{aligned} \tag{70}$$

$$M_T^{(i)} = E_i \int_0^h \alpha_i (T_i)\, T_i\, z\, dz \quad , \qquad N_T^{(i)} = E_i \int_0^h \alpha_i (T_i)\, T_i\, dz \tag{71}$$

Here $\alpha_i (T_i)$ is the temperature dependent coefficient of linear thermal expansion assumed as:

$$\alpha_i (T_i) = \alpha_{i0} \exp(\varpi_2 T_i), \; \varpi_2 \geq 0 \tag{72}$$

Here α_{i0} is the dimensionless reference value of coefficient of linear thermal expansion defined by, $\alpha_{i0}{}^* = \dfrac{\alpha_{i0}}{\alpha_{(i-1)0}}$. Using Eqs. (61) and (72), in Eq. (71), the thermally induced resultant moments $M_T^{(i)}$ and $N_T^{(i)}$ of the *i*th layer, are obtained as:

$$M_T^{(i)} = (\alpha_i\, E_i / \lambda_{i0}) \sum_{n=1}^{\infty} \Psi_5 \{ \sum_{p=1}^{\infty} \Psi_2 S_{i0p}(r) + \sum_{m=1}^{\infty}\sum_{p=1}^{\infty} \Psi_3 S_{imp}(r)\cos(m\theta) + \sum_{m=1}^{\infty}\sum_{p=1}^{\infty} \Psi_4 S_{imp}(r)\sin(m\theta)\} \tag{73}$$

$$N_T^{(i)} = (\alpha_i\, E_i / \lambda_{i0}) \sum_{n=1}^{\infty} \Psi_6 \{ \sum_{p=1}^{\infty} \Psi_2 S_{i0p}(r) + \sum_{m=1}^{\infty}\sum_{p=1}^{\infty} \Psi_3 S_{imp}(r)\cos(m\theta) + \sum_{m=1}^{\infty}\sum_{p=1}^{\infty} \Psi_4 S_{imp}(r)\sin(m\theta)\} \tag{74}$$

where

$$\begin{aligned} \Psi_5 &= [(h^2/24n^2\pi^2)][(-3n\pi(8+3\varpi_2^2)\cos(n\pi) + \varpi_2(3+6n^2\pi^2 - 3\cos(2n\pi) + n\pi\varpi_2\cos(3n\pi))], \\ \Psi_6 &= [(h/24n\pi)][24 + 12n\pi\varpi_2 + 8\varpi_2^2 - 3(8+3\varpi_2^2)\cos(n\pi) + \varpi_2^2\cos(3n\pi)] \end{aligned}$$

Using Eq. (73), the deflection $w^{(i)}$ of the *i*th layer from Eq. (62) is obtained as:

© 2023 IAU, Arak Branch

$$w^{(i)} = (12(1+\nu)\alpha_i\ \Psi_5 / \lambda_{i0} h^3) \times [(\Phi_1 + \Phi_2 + \Phi_3)/(\Phi_1 + ((m^2 + r^2)/r^2)\Phi_2 + ((m^2 + r^2)/r^2)\Phi_3) \times \sum_{n=1}^{\infty} \{\Phi_1 S_{i0p}(r) + \Phi_2 S_{imp}(r) + \Phi_3 S_{imp}(r)\} \tag{75}$$

where

$$\Phi_1 = \sum_{p=1}^{\infty} \Psi_2,$$

$$\Phi_2 = \sum_{m=1}^{\infty} \sum_{p=1}^{\infty} \Psi_3 \cos(m\theta),$$

$$\Phi_3 = \sum_{m=1}^{\infty} \sum_{p=1}^{\infty} \Psi_4 \sin(m\theta)$$

Using Eqs. (73) and (75), the components of resultant moments from Eq. (68) and stress components from Eq. (70) are determined using Mathematica software.

4 NUMERICAL RESULTS AND DISCUSSION

For numerical computations are carried out for a three-layered annular disk by choosing copper as the inner layer, zinc as the middle layer and aluminium as the outer layer. The material properties of Copper, Zinc and Aluminium are taken as given below in Table 1.

Table 1
Thermo-mechanical properties of Copper, Zinc and Aluminium at room temperature.

Property	Copper (Cu)	Zinc (Zn)	Aluminium (Al)
Thermal conductivity λ_i $[W/(cmC)]$	3.86	1.13	2.04
Thermal diffusivity κ_i $[cm^2/s]$	1.11	1.12	0.97
Thermal expansion coefficient α_i $[\times 10^{-6}/C]$	16.6	29.7	22.2
Young's modulus E_i $[N/cm^2]$	11.7×10^6	8.27×10^6	6.9×10^6
Poisson's ratio ν_i	0.36	0.25	0.33

For numerical computations, we take surrounding temperature $T_0 = 20$, $r_0 = 1, r_1 = 2,\ r_2 = 3, r_3 = 4$, inner layer $r_0 < r < r_1$, middle layer $r_1 < r < r_2$, outer layer $r_2 < r < r_3$.

Figs. 2(a), 2(b), 2(c) show the variation of dimensionless temperature along θ, z, r respectively in three different layers viz. inner layer (Copper), middle layer (Zinc) and outer layer (Aluminium). It is seen that the temperature is higher in the outer layer due to the application of heat, moderate in the middle layer and is decreasing slowly towards the inner layer.

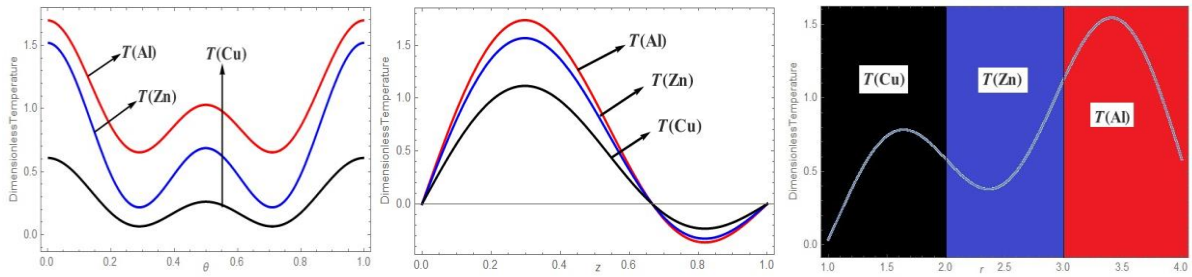

Fig.2
a) Plot of temperature along θ, b) Plot of temperature along *z*, c) Plot of temperature along *r*.

© 2023 IAU, Arak Branch

The following Figs. (3 to 7) show the variations of dimensionless deflection, resultant moments and thermal stresses. The figures on the left are plotted for the homogeneous case (i.e. taking $\varpi_1 = \varpi_2 = 0$, so that the material properties become independent of temperature), whereas that on the right are plotted for the nonhomogeneous case (i.e. taking $\varpi_1 \neq 0, \varpi_2 \neq 0$, so that the material properties become dependent temperature).

Figs. 3(a), 3(b) show the sinusoidal nature of dimensionless deflection along θ, r respectively. The magnitude of deflection is slowly increasing with increase in θ and decreases towards the end after attaining peak. Along radial direction deflection becomes peak in the outer layer and gradually decreases towards the inner layer.

Figs. 4(a), 4(b), 5(a), 5(b) represent the graphs of dimensionless resultant moments along θ, r. Along θ the moments are compressive in nature, while along radial direction they are seen to be tensile in the outer layer and become compressive towards the inner layer.

Figs. 6(a), 6(b), 6(c) gives the variation of dimensionless tangential stress $\sigma_{\theta\theta}$, while Figs. 7(a), 7(b), 7(c) gives the variation of dimensionless radial stress σ_{rr} along θ, z, r. The nature is observed to be sinusoidal along θ, while linear along z. The magnitude increases with increase in θ and z and the stress is tensile in nature. Along radial direction the stress is tensile in the outer and middle layers while becomes compressive in the inner core. The radial stress becomes compressive in the inhomogeneous case in the middle region and attains tensile nature towards the inner layer.

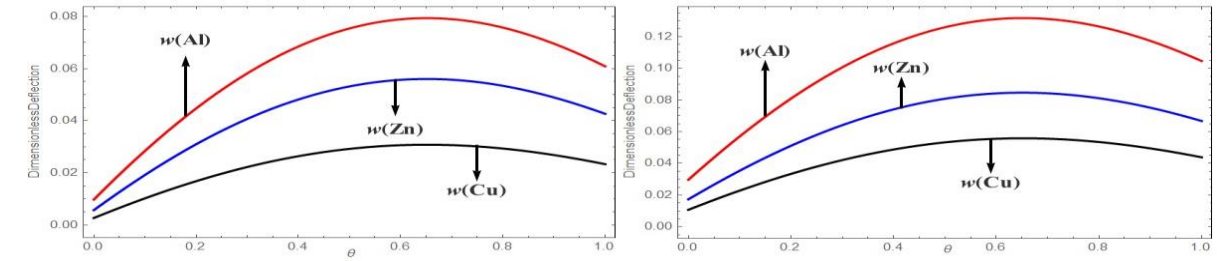

(a)

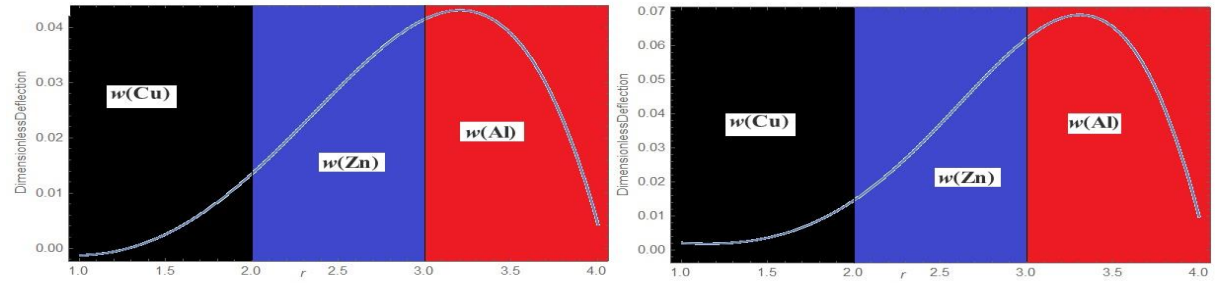

(b)

Fig.3
a) Plot of deflection along θ. b) Plot of deflection along r.

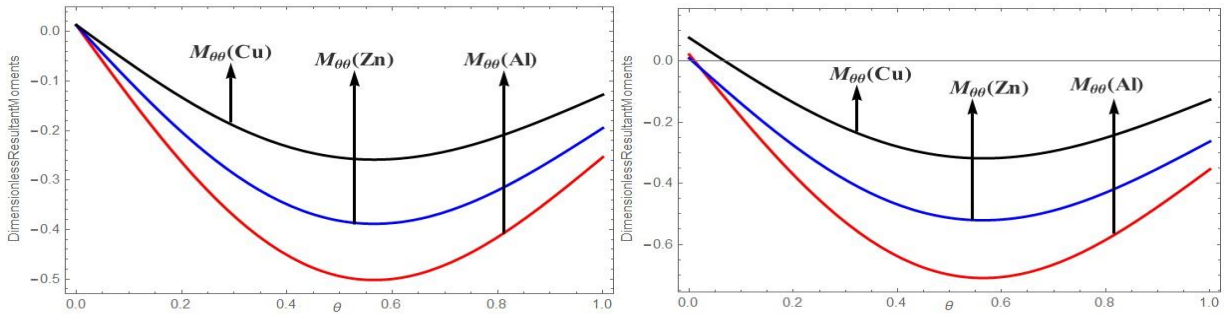

(a)

© 2023 IAU, Arak Branch

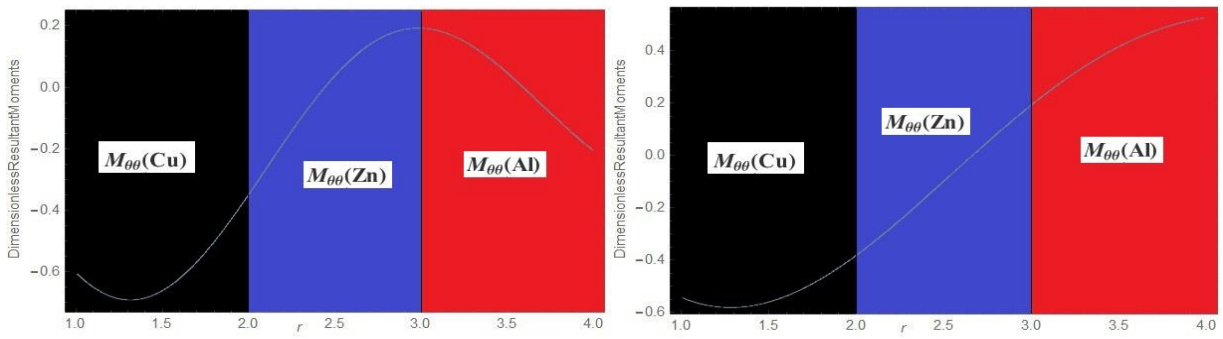

(b)

Fig.4

a) Plot of $M_{\theta\theta}$ along θ . b) Plot of $M_{\theta\theta}$ along *r*.

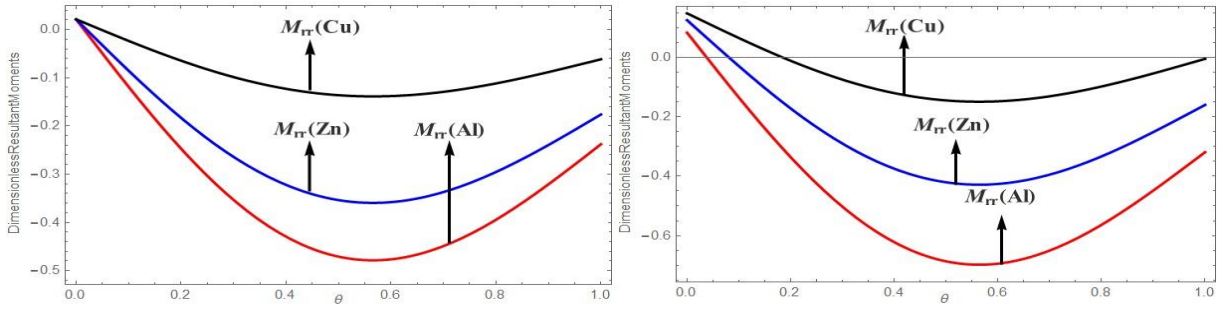

(a)

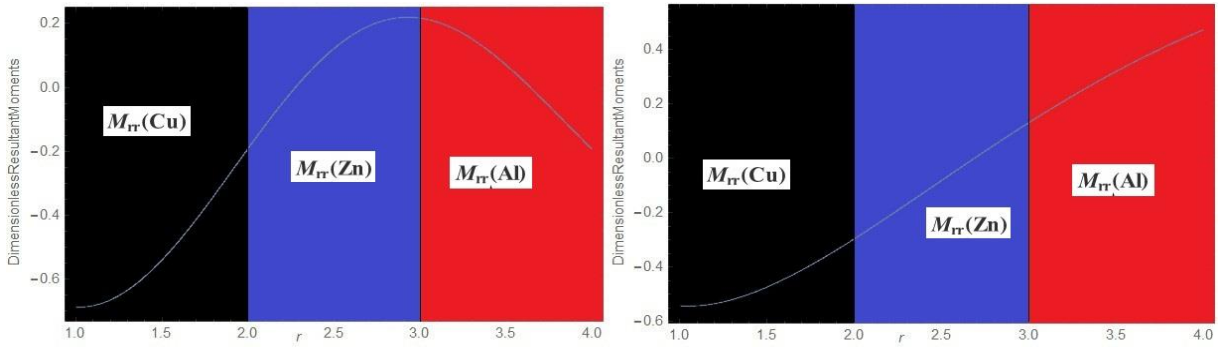

(b)

Fig.5

a) Plot of M_{rr} along θ . b) Plot of M_{rr} along *r*.

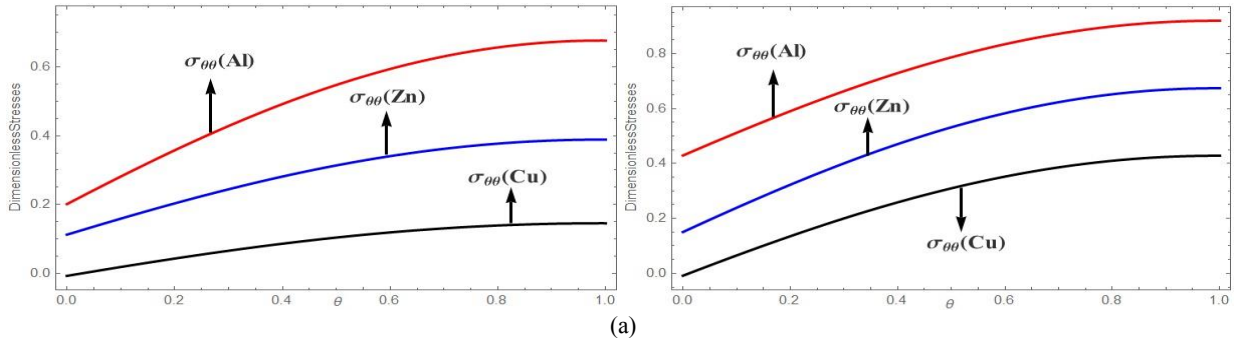

(a)

© 2023 IAU, Arak Branch

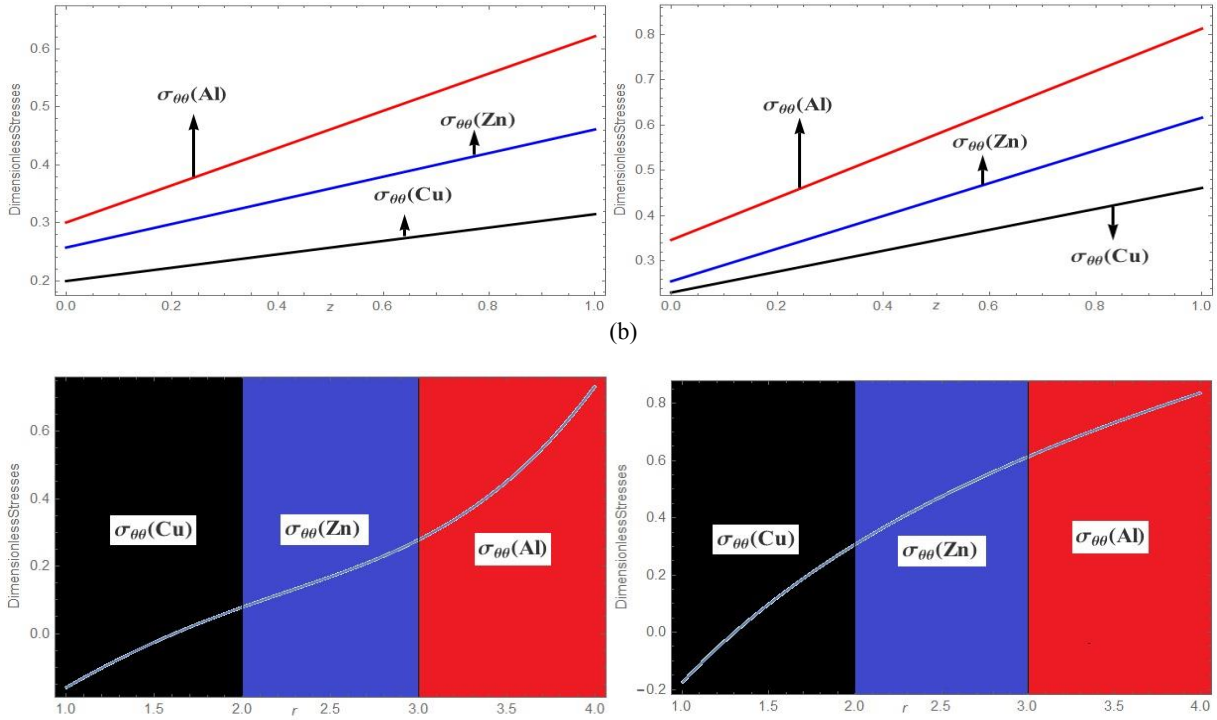

(b)

(c)

Fig.6

a) Plot of $\sigma_{\theta\theta}$ along θ . b) Plot of $\sigma_{\theta\theta}$ along z. c) Plot of $\sigma_{\theta\theta}$ along r.

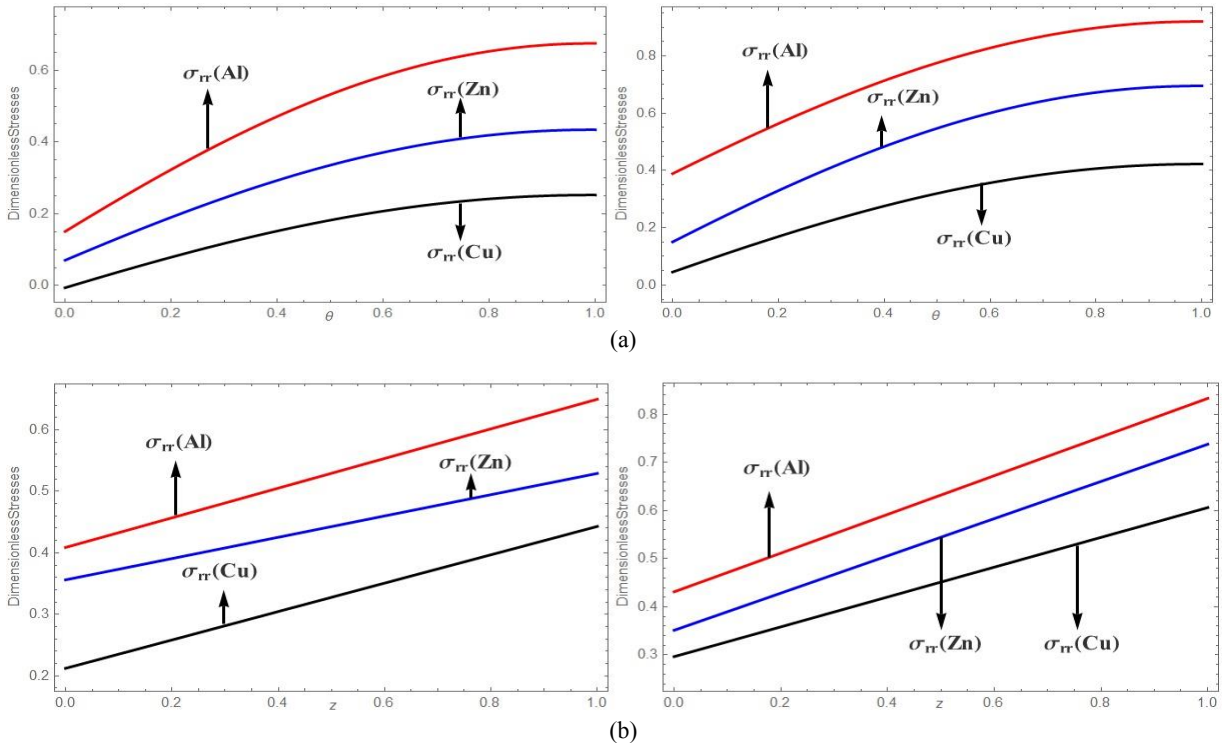

(a)

(b)

© 2023 IAU, Arak Branch

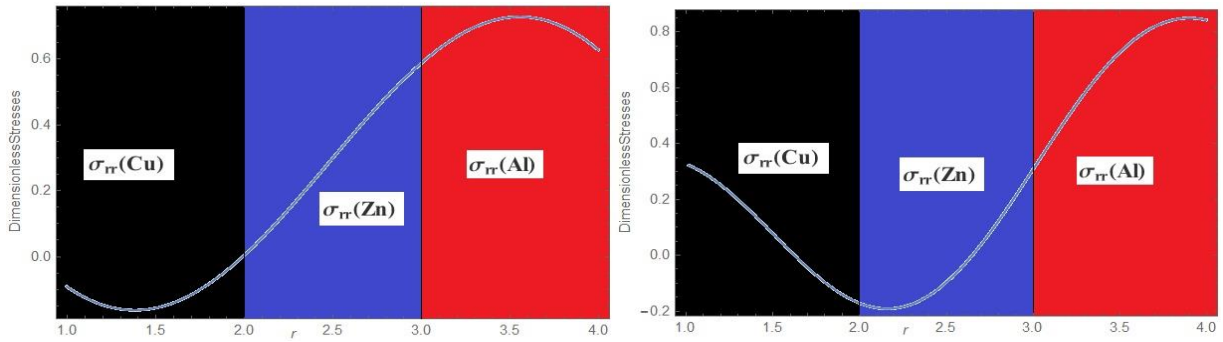

(c)

Fig.7

a) Plot of σ_{rr} along θ . b) Plot of σ_{rr} along *z*. c): Plot of σ_{rr} along *r*.

5 VALIDATION OF THE RESULTS

In this paper, a mathematical model has been prepared for a multilayered thin annular circular disk by taking temperature dependent material properties. The temperature profile and its corresponding deflection, resultant moments thermal stress distributions are obtained. As a limiting case, if we consider homogeneous material properties with internal heat generation, the results agree with [21].

6 CONCLUSION

In this paper, the temperature profile of a nonhomogeneous multilayered annular disk with convective heating on the outer layer is investigated. The material properties are taken to be temperature dependent. The nonlinear heat conduction equation is solved using Kirchhoff's variable transformation, finite Hankel transform and Fourier series with time dependent boundary conditions. Thermal behavior is studied for a simply supported multilayered annular disk using resultant forces, shearing forces and resultant moments. Numerical computations are carried out for a three-layered annular disk in which copper is selected as the inner layer, zinc as the middle layer and aluminium as the outer layer. It is observed that, due to the application of convective heating at the outer layer, the temperature rises and gradually decreases towards the inner layer. The resultant moments are compressive along θ, while along radial direction they are seen to be tensile in the outer and middle layers and become compressive in the inner layer. The application of third kind boundary condition at the outer layer produces heat which is transferred from the outer layer towards the inner layer. Thermal energy is accumulated in and around the outer and middle layers which slowly reduces towards the inner layer causing the nature to change from tensile to compressive. The magnitude of tangential and radial stresses is increasing with increase in θ, z, r. Thermally sensitive material properties play a vital role in the thermal profile of the considered multilayered disk. The magnitude is more in the nonhomogeneous case as compared to that of the homogeneous case. In the temperature dependent case, the radial stress suddenly becomes compressive in the middle region, whereas it is tensile throughout all the regions in the temperature independent case. Due to the inhomogeneous thermal conductivity considered in the form of exponential function, the temperature and the corresponding thermoelastic quantities shows the lag along radial direction.

REFERENCES

[1] Noda N., 1986, Thermal stresses in materials with temperature dependent properties, *Thermal Stresses* **241**: 391-483.

[2] Olcer N.Y., 1968, A general unsteady heat flow problem in a finite composite hollow circular cylinder under boundary conditions of second kind, *Nuclear Engineering and Design* **7**(2): 97-112.

[3] Gorman D.G., 1985, Thermal gradient effects upon the vibrations of certain composite circular plates, Part I: Plane Orthotropic, *Journal of Sound and Vibration* **101**(3): 325-336.

[4] Popovych V.S., Fedai B.N., 1997, The axisymmetric problem of thermoelasticity of a multilayer thermosensitive tube, *Journal of Mathematical Sciences* **86**: 2605-2610.

© 2023 IAU, Arak Branch

[5] Popovych V.S., Makhorkin I.M., 1998, On the solution of heat conduction problems for thermosensitive bodies, *Journal of Mathematical Sciences* **88**: 352-359.
[6] Malzbender J., Jülich F., 2004, Mechanical and thermal stresses in multilayered materials, *Journal of Applied Physics* **95**(4): 1780-1782.
[7] Kayhani M., Nourouzi M., Delooei A.A., 2010, An exact solution of axi-symmetric conductive heat transfer in cylindrical composite laminate under the general boundary condition, *International Journal of Mechanical, Aerospace, Industrial, Mechatronic and Manufacturing Engineering* **4**: 776-783.
[8] Singh S., 2010, Analytical solution of time-dependent multilayer heat conduction problems for nuclear applications, *Proceedings of the 1st International Nuclear and Renewable Energy Conference (INREC10), Amman, Jordan*.
[9] Singh S., Jain P., Rizwan-uddin, 2011, Finite integral transform method to solve asymmetric heat conduction in a multilayer annulus with time-dependent boundary conditions, *Nuclear Engineering and Design* **241**(1): 144-154.
[10] Kayhani M., Nourouzi M., Delooei A.A., 2012, A general analytical solution for heat conduction in cylindrical multilayer composite laminates, *International Journal of Thermal Sciences* **52**: 73-82.
[11] Norouzi M., Delooei A.A., and Seilsepour M., 2013, A general exact solution for heat conduction in multilayer spherical composite laminates, *Composite Structures* **106**: 288-295.
[12] Dalir N., Nourazar S.S., 2014, Analytical solution of the problem on the three-dimensional transient heat conduction in a multilayer cylinder, *Journal of Engineering Physics and Thermophysics* **87**: 89-97.
[13] Popovych V.S., Kalynyak B.M., 2016, Mathematical modeling and methods for the determination of the static thermoelastic state of multilayer thermally sensitive cylinders, *Journal of Mathematical Sciences* **215**: 218-242.
[14] Torabi M., Zhang K., 2016, Analytical solution for transient temperature and thermal stresses within convective multilayer disks with time-dependent internal heat generation, Part I: Methodology, *Journal of Thermal Stresses* **39**(4): 398-413.
[15] Manthena V.R., Lamba N.K., Kedar G.D., 2017, Thermal stress analysis in a functionally graded hollow elliptic-cylinder subjected to uniform temperature distribution, *Applications and Applied Mathematics* **12**(1): 613-632.
[16] Manthena V.R., Lamba N.K., Kedar G.D., 2017, Thermoelastic analysis of a nonhomogeneous hollow cylinder with internal heat generation, *Applications and Applied Mathematics* **12**(2): 946-967.
[17] Bhad P.P., Varghese V., Khalsa L., 2017, Heat production in a simply supported multilayer elliptic annulus composite plate and its associated thermal stresses, *Journal of Stress Analysis* **2**(2): 55-67.
[18] Wang Y.Z., Liu D., Wang Q., Zhou J.Z., 2018, Thermoelastic interaction in functionally graded thick hollow cylinder with temperature-dependent properties, *Journal of Thermal Stresses* **41**(4): 399-417.
[19] Manthena V.R., Kedar G.D., 2018, Transient thermal stress analysis of a functionally graded thick hollow cylinder with temperature dependent material properties, *Journal of Thermal Stresses* **41**(5): 568-582.
[20] Manthena V.R., 2019, Uncoupled thermoelastic problem of a functionally graded thermosensitive rectangular plate with convective heating, *Archive of Applied Mechanics* **89**(8): 1627-1639.
[21] Manthena V.R., Srinivas V.B., Kedar G.D., 2020, Analytical solution of heat conduction of a multilayered annular disk and associated thermal deflection and thermal stresses, *Journal of Thermal Stresses* **43**(5): 563-578.
[22] Singh R.V., Mukhopadhyay S., 2020, An investigation on strain and temperature rate-dependent thermoelasticity and its infinite speed behavior, *Journal of Thermal Stresses* **43**(3): 269-283.
[23] Zenkour A.M., 2020, Thermal-shock problem for a hollow cylinder via a multi-dual-phase-lag theory, *Journal of Thermal Stresses* **43**(6): 687-706.
[24] Bhoyar S., Varghese V., Khalsa L., 2021, Axisymmetric thermoelastic response in a semi-elliptic plate with Kassir's nonhomogeneity in the thickness direction, *Applications and Applied Mathematics* **16**(1): 481-502.
[25] Bawankar L.C., Kedar G.D., 2021, Memory response of magneto-thermoelastic problem due to the influence of modified Ohm's law, *Applications and Applied Mathematics* **16**(1): 503-523.
[26] Gheisari M., Najafizadeh M.M., Nezamabadi A.R., Jafari S., Yousefi, P., 2021, Thermal buckling analysis of porous conical shell on elastic foundation, *Journal of Solid Mechanics* **13**(1): 37-53.
[27] Dehghanpour S., Nezamabadi A.R., Attar M.M., Barati F., Tajdari M., 2021, Experimental and numerical investigation on geometric parameters of aluminum patches for repairing cracked parts by diffusion method, *Journal of Solid Mechanics* **13**(1): 54-67.
[28] Adolfsson E., 2021, Steady-periodic thermal stresses in an infinite hollow compound cylinder, *Journal of Thermal Stresses* **44**(9): 1150-1168.
[29] Mahakalkar A., Varghese V., 2021, Thermoelastic analysis of annular sector plate under restricted boundaries amidst elastic reaction, *Journal of Solid Mechanics* **13**(3): 325-337.
[30] Mirparizi M., Shariyat M., Fotuhi A.R., 2021, Large deformation hermitian finite element coupled thermoelasticity analysis of wave propagation and reflection in a finite domain, *Journal of Solid Mechanics* **13**(4): 485-502.
[31] Hosseini M., Arani A.G., Karamizadeh M., Niknejad Sh., Hosseinpour A., 2022, Static and dynamic stability analysis of thick CNT reinforced beams resting on pasternak foundation under axial and follower forces, *Journal of Solid Mechanics* **14**(1): 1-16.
[32] Keshavarzian M., Najafizadeh M.M.,Khorshidi K., Yousefi P., Alavi M., 2022, Improved high-order analysis of linear vibrations of a thick sandwich panel with an electro-rheological core by using exponential shear deformation theory, *Journal of Solid Mechanics* **14**(1): 37-56.

© 2023 IAU, Arak Branch

[33] Eslami M.R., Jabbari M., Sabet A.E., 2022, Elasticity exact solution for an FGM cylindrical shaft with piezoelectric layers under the saint-venant torsion by using prandtl's formulation, *Journal of Solid Mechanics* **14**(2): 147-170.

[34] Arani A.G., Niknejad Sh.,Mihankhah A., Safari I., 2022, Dynamic stability analysis of bi-directional functionally graded beam with various shear deformation theories under harmonic excitation and thermal environment, *Journal of Solid Mechanics* **14**(3): 272-290.

[35] Noda N., Hetnarski R.B., Tanigawa Y., 2003, *Thermal Stresses*, Taylor & Francis, New York.

© 2023 IAU, Arak Branch